VOLUME-PRESERVING CORRECTION FOR IMAGE REGISTRATION USING FREE-FORM DEFORMATIONS

P. Faltin[⋆]*, K. Chaisaowong*[⋆†]*, T. Aach*[⋆]

[⋆]Institute of Imaging and Computer Vision, RWTH Aachen University, Germany
[†]King Mongkut's University of Technology North Bangkok, Thailand

ABSTRACT

Registration of an image non-rigidly to another one causes deformations, which generally do not preserve the initial volume. Volume preservation is however indispensable for observing tumors in medical images. This paper presents the correction of B-spline based registration to preserve the volume in observed regions. In contrast to other approaches, our solution is not obtained through energy minimization, but by calculating the correction parameters for the deformation directly. Especially for high resolution image data this strategy is very efficient in terms of computational expenses. We derive a closed form solution to optimize the registration with respect to the compression at a single point and then extend the problem to multiple points. Finally we prove also that the correction terms do not have any significant influence on the registration quality.

Index Terms— B-spline, free-form deformation, non-rigid registration, volume preservation

1. INTRODUCTION

Image registration for high resolution 3D images is a computationally intensive task. Especially for the non-rigid part many versatile algorithms use an iterative approach to optimize the registration [1]. On workstations these algorithms perform at a runtime which does not suffice the requirements for interactive software. Non-iterative algorithms adapted to an individual registration problem, e.g. the lung surface proximity of thoracic CT images [2, 3], provide the necessary performance. Enforcing a volume-preserving deformation however often results in a non-linear equation system [4, 5, 6] which require iterative optimization. In this paper we present a direct method to compute a correction term for B-spline based deformation.

In order to achieve an efficient work-flow, first feature points are calculated and matched (fig. 1(a)), the control points (CPs) for the non-rigid registration are calculated using e.g. [7] (fig. 1(b)) and finally the CPs are corrected with the presented method (fig. 1(c)).

2. METHOD

An image which is non-rigidly transformed by $\boldsymbol{T}$ might be subject to space dependent compression. A widely used metrics [8, 5] to measure the compression for a 3D image point $\boldsymbol{r}$ is the determinant of the Jacobian matrix of the transformation

$$J_T(\boldsymbol{r}) = \det \begin{pmatrix} \frac{\partial T_x(\boldsymbol{r})}{\partial x}, \frac{\partial T_x(\boldsymbol{r})}{\partial y}, \frac{\partial T_x(\boldsymbol{r})}{\partial z} \\ \frac{\partial T_y(\boldsymbol{r})}{\partial x}, \frac{\partial T_y(\boldsymbol{r})}{\partial y}, \frac{\partial T_y(\boldsymbol{r})}{\partial z} \\ \frac{\partial T_z(\boldsymbol{r})}{\partial x}, \frac{\partial T_z(\boldsymbol{r})}{\partial y}, \frac{\partial T_z(\boldsymbol{r})}{\partial z} \end{pmatrix}. \tag{1}$$

In order to achieve a compression-free deformation, $J_T(\boldsymbol{r})$ has to be equal 1 [5].

2.1. Free-form deformations

In this paper we discuss this strategy in the context of a B-spline based non-rigid registration, where the transformation $\boldsymbol{T}$ of each point $\boldsymbol{r} = (x, y, z)^T$ in the image is interpolated using B-Splines [1]. In this paper $\boldsymbol{T}$ maps $\boldsymbol{r}$ to the absolute transformed coordinate and not to an offset [5]. A grid of $N_x \times N_y \times N_z$ CPs $\boldsymbol{\phi_n} = (\phi^x_{\boldsymbol{n}}, \phi^y_{\boldsymbol{n}}, \phi^z_{\boldsymbol{n}})^T \in \mathbb{R}^3$, with $\boldsymbol{n} = (n_x, n_y, n_z) \in \mathbb{Z}^3$, $-1 \leqslant n_x < (N_x - 1), -1 \leqslant n_y < (N_y - 1), -1 \leqslant n_z < (N_z - 1)$ is used to calculate the transformation $\boldsymbol{T}(\boldsymbol{r})$ for all other points

$$\boldsymbol{T}(\boldsymbol{r}) = \sum_{l=0}^{3}\sum_{m=0}^{3}\sum_{n=0}^{3} B_l(u)B_m(v)B_n(w)\boldsymbol{\phi}_{\mu+l,\nu+m,\xi+n}, \tag{2}$$

with grid spacing δ_x, δ_y and δ_z and $\mu = \left\lfloor \frac{x}{\delta_x} \right\rfloor - 1$, $\nu = \left\lfloor \frac{y}{\delta_y} \right\rfloor - 1$, $\xi = \left\lfloor \frac{z}{\delta_z} \right\rfloor - 1$, $u = \frac{x}{\delta_x} - \left\lfloor \frac{x}{\delta_x} \right\rfloor$, $v = \frac{y}{\delta_y} - \left\lfloor \frac{y}{\delta_y} \right\rfloor$, $w = \frac{z}{\delta_z} - \left\lfloor \frac{z}{\delta_z} \right\rfloor$. $B_c(s)$ is the c-th basis function of the cubic and uniform B-spline

$$\begin{aligned} B_0(s) &= \tfrac{(1-s)^3}{6}, & B_1(s) &= \tfrac{3s^3-6s^2+4}{6}, \\ B_2(s) &= \tfrac{-3s^3+3s^2+3s+1}{6}, & B_3(s) &= \tfrac{s^3}{6}. \end{aligned} \tag{3}$$

2.2. Volume-preservation

To calculate the Jacobian matrix from eq. 1 the derivatives $\frac{dB_i(s)}{ds}$ of the B-spline are required, which can be determined

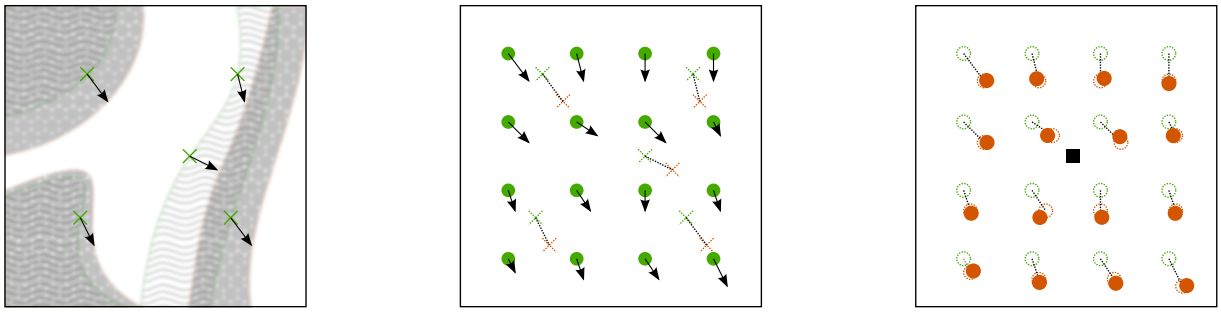

(a) Feature points (green crosses) from one image are matched (arrows) to the corresponding points in the other image.

(b) The offsets (dotted lines) obtained from the matched points (the dotted crosses) are used to determine the offsets (arrows) of control points (green filled circles).

(c) A correction adjusts the control points (dotted orange circles) to eliminate the compression at the regarded pixel (black square) and results in new control points (orange filled circles).

Fig. 1. Steps applied for a volume preserving, non-rigid registration of two images. Each image contains the information from the last step (dotted) and distinguishes between unregistered image (green) and registered image (orange).

analytically. For a shorter notation we denote the values (u, v, w) as the vector $\boldsymbol{u}$ and the values (μ, ν, ξ) as the vector $\boldsymbol{\mu}$. Additionally we introduce the three dimensional index vectors $\boldsymbol{o}, \boldsymbol{p}, \boldsymbol{q} \in \boldsymbol{W}$, with $\boldsymbol{W} = \{(l, m, n) : \forall l, m, n\ 0 \leq l, m, n \leq 3\} = \{(0,0,0), (0,0,1), ..., (3,3,3)\}$ to address the B-spline functions from eq. 3. The combination of the three independent B-splines for a derivative with respect to x is denoted by

$$\hat{B}^x_{\boldsymbol{o}}(\boldsymbol{u}) = \frac{1}{\delta_x} \frac{dB_l(u)}{du} B_m(v) B_n(w), \tag{4}$$

with $\boldsymbol{o} = (l, m, n)$. $\hat{B}^y_{\boldsymbol{o}}(\boldsymbol{u})$ and $\hat{B}^z_{\boldsymbol{o}}(\boldsymbol{u})$ are given analogously. Using this notation, the determinant of the Jacobian can be written in the following form [8]

$$J_T(\boldsymbol{r}) = \sum_{\boldsymbol{o}\in\boldsymbol{W}} \sum_{\boldsymbol{p}\in\boldsymbol{W}} \sum_{\boldsymbol{q}\in\boldsymbol{W}} c_{\boldsymbol{o},\boldsymbol{p},\boldsymbol{q}}(\boldsymbol{u}) \phi^x_{\boldsymbol{o}+\boldsymbol{\mu}} \phi^y_{\boldsymbol{p}+\boldsymbol{\mu}} \phi^z_{\boldsymbol{q}+\boldsymbol{\mu}}, \tag{5}$$

with

$$c_{\boldsymbol{o},\boldsymbol{p},\boldsymbol{q}}(\boldsymbol{u}) = \det \begin{pmatrix} \hat{B}^x_{\boldsymbol{o}}(\boldsymbol{u}), \hat{B}^x_{\boldsymbol{p}}(\boldsymbol{u}), \hat{B}^x_{\boldsymbol{q}}(\boldsymbol{u}) \\ \hat{B}^y_{\boldsymbol{o}}(\boldsymbol{u}), \hat{B}^y_{\boldsymbol{p}}(\boldsymbol{u}), \hat{B}^y_{\boldsymbol{q}}(\boldsymbol{u}) \\ \hat{B}^z_{\boldsymbol{o}}(\boldsymbol{u}), \hat{B}^z_{\boldsymbol{p}}(\boldsymbol{u}), \hat{B}^z_{\boldsymbol{q}}(\boldsymbol{u}) \end{pmatrix}. \tag{6}$$

Only discrete positions of $\boldsymbol{u}$ are controlled for their compression, therefore $c_{\boldsymbol{o},\boldsymbol{p},\boldsymbol{q}}(\boldsymbol{u})$ could be pre-calculated. The number of different values for $c_{\boldsymbol{o},\boldsymbol{p},\boldsymbol{q}}(\boldsymbol{u})$ is $4^9 \cdot N_x \cdot N_y \cdot N_z$. These values might be efficiently calculated for small grid spacing, but not for large grid spacing. Another important parameter is the number of points for those compression should be actually optimized. Depending on these parameters a pre-calculation might be useful.

Instead of solving an energy minimization problem as in other approaches [4, 5, 8], which can be computationally intensive, we use a fast approximation algorithm to determine CPs which eliminate the compression.

2.3. Volume-preserving correction

The CPs are corrected by the offsets $\boldsymbol{d_n} = (d^x_{\boldsymbol{n}}, d^y_{\boldsymbol{n}}, d^z_{\boldsymbol{n}})^T$, which results in the new CPs $\boldsymbol{\phi_n} = \tilde{\boldsymbol{\phi}}_{\boldsymbol{n}} + \boldsymbol{d_n}$. Insert this into eq. 5 and require the determinant to equal 1 results in

$$\begin{aligned} J_T(\boldsymbol{r}) = &\sum_{\boldsymbol{o}\in\boldsymbol{W}} \sum_{\boldsymbol{p}\in\boldsymbol{W}} \sum_{\boldsymbol{q}\in\boldsymbol{W}} c_{\boldsymbol{o},\boldsymbol{p},\boldsymbol{q}}(\boldsymbol{u}) \cdot \\ &(\tilde{\phi}^x_{\boldsymbol{o}+\boldsymbol{\mu}} + d^x_{\boldsymbol{o}+\boldsymbol{\mu}})(\tilde{\phi}^y_{\boldsymbol{p}+\boldsymbol{\mu}} + d^y_{\boldsymbol{p}+\boldsymbol{\mu}})(\tilde{\phi}^z_{\boldsymbol{q}+\boldsymbol{\mu}} + d^z_{\boldsymbol{q}+\boldsymbol{\mu}}) = 1. \end{aligned} \tag{7}$$

The initial registration is only obtained, if the length of the corrections term $\boldsymbol{d_n}$ is sufficiently small. This will be enforced by eq. 13 and therefore $d^x_{\boldsymbol{n}}, d^y_{\boldsymbol{n}}, d^z_{\boldsymbol{n}} \ll \tilde{\phi}^x_{\boldsymbol{n}}, \tilde{\phi}^y_{\boldsymbol{n}}, \tilde{\phi}^z_{\boldsymbol{n}}$. According to this condition, all terms containing multiple multipliers $d^x_{\boldsymbol{n}}$, $d^y_{\boldsymbol{n}}$ or $d^z_{\boldsymbol{n}}$ can be dismissed which leads to

$$\begin{aligned} &\sum_{\boldsymbol{o}\in\boldsymbol{W}} {d^x_{\boldsymbol{o}+\boldsymbol{\mu}}}^T \theta^x_{\boldsymbol{o},\boldsymbol{\mu}}(\boldsymbol{u}) + \\ &\sum_{\boldsymbol{p}\in\boldsymbol{W}} {d^y_{\boldsymbol{p}+\boldsymbol{\mu}}}^T \theta^y_{\boldsymbol{p},\boldsymbol{\mu}}(\boldsymbol{u}) + \\ &\sum_{\boldsymbol{q}\in\boldsymbol{W}} {d^z_{\boldsymbol{q}+\boldsymbol{\mu}}}^T \theta^z_{\boldsymbol{q},\boldsymbol{\mu}}(\boldsymbol{u}) \approx g(\boldsymbol{u}). \end{aligned} \tag{8}$$

with

$$\theta^x_{\boldsymbol{o},\boldsymbol{\mu}}(\boldsymbol{u}) = \sum_{\boldsymbol{p}\in\boldsymbol{W}} \sum_{\boldsymbol{q}\in\boldsymbol{W}} \tilde{\phi}^y_{\boldsymbol{p}+\boldsymbol{\mu}} \tilde{\phi}^z_{\boldsymbol{q}+\boldsymbol{\mu}} c_{\boldsymbol{o},\boldsymbol{p},\boldsymbol{q}}(\boldsymbol{u}). \tag{9}$$

$\theta^y_{\boldsymbol{p},\boldsymbol{\mu}}(\boldsymbol{u})$ and $\theta^z_{\boldsymbol{q},\boldsymbol{\mu}}(\boldsymbol{u})$ are calculated analogously and

$$g(\boldsymbol{u}) = 1 - \sum_{\boldsymbol{o}\in\boldsymbol{W}} \sum_{\boldsymbol{p}\in\boldsymbol{W}} \sum_{\boldsymbol{q}\in\boldsymbol{W}} \tilde{\phi}^x_{\boldsymbol{o}+\boldsymbol{\mu}} \tilde{\phi}^y_{\boldsymbol{p}+\boldsymbol{\mu}} \tilde{\phi}^z_{\boldsymbol{q}+\boldsymbol{\mu}} c_{\boldsymbol{o},\boldsymbol{p},\boldsymbol{q}}(\boldsymbol{u}). \tag{10}$$

Eq. 8 can also be written in the form

$$\boldsymbol{d}^T \cdot \boldsymbol{\theta}(\boldsymbol{u}) \approx g(\boldsymbol{u}), \tag{11}$$

where all involved values are aligned in vectors, denoted by the operator $\leftrightarrows$,

$$\begin{aligned} \boldsymbol{d} &\leftrightarrows \{(d^x_{\boldsymbol{o}+\boldsymbol{\mu}}, d^y_{\boldsymbol{o}+\boldsymbol{\mu}}, d^z_{\boldsymbol{o}+\boldsymbol{\mu}}) : \forall \boldsymbol{o} \in \boldsymbol{W}\}, \\ \boldsymbol{\theta}(\boldsymbol{u}) &\leftrightarrows \{(\theta^x_{\boldsymbol{o},\boldsymbol{\mu}}(\boldsymbol{u}), \theta^y_{\boldsymbol{o},\boldsymbol{\mu}}(\boldsymbol{u}), \theta^z_{\boldsymbol{o},\boldsymbol{\mu}}(\boldsymbol{u})) : \forall \boldsymbol{o} \in \boldsymbol{W}\}. \end{aligned} \tag{12}$$

Eq. 11 illustrates that values of $\boldsymbol{d}$ are approximately located on a $4^3 \cdot 3 = 192$-dimensional hyperplane. The equation is only valid for small length of $\boldsymbol{d}$. The point with the smallest Euclidean distance of $\boldsymbol{d}$ and satisfying eq. 8 is given by

$$\boldsymbol{d'}(\boldsymbol{u}) = \frac{g(\boldsymbol{u}) \cdot \boldsymbol{\theta}(\boldsymbol{u})}{\|\boldsymbol{\theta}(\boldsymbol{u})\|_2^2}, \tag{13}$$

which is the closest point on the plane to the origin.

2.4. Correction for multiple points

Eq. 13 calculates the correction for one single point $\boldsymbol{r} \mapsto \boldsymbol{u}$ only. Generally the volume-preservation should be enforced in multiple regions and therefore for multiple points. Depending on the number N of these observed points $\boldsymbol{x}_i$ $\forall i = 1...N$ in one grid cell, the problem can be under- or over-determined. Even for the under-determined case a solution solving eq. 13 for all points $\boldsymbol{x}_i$ might not be reasonable. Such a solution does not necessarily result in small lengths of $\boldsymbol{d}$, which was assumed and is important to obtain the initial registration. Therefore we suggest to cross-check all solutions $\boldsymbol{d'}(\boldsymbol{u}_i)$ $\forall i = 1...N$ and to choose the solution $\boldsymbol{x}_b$ minimizing the overall error with

$$b = \arg\left\{ \min_{i=1...N} \left\{ \sum_{j=1}^{N} a_i \cdot e(i,j) \right\} \right\}. \tag{14}$$

The weights a_i can be chosen individually for each observed point, and the error per point is given by

$$e(i,j) = \left\| \boldsymbol{d'}^T(\boldsymbol{u}_i)\boldsymbol{\theta}(\boldsymbol{u}_j) - g(\boldsymbol{u}_j) \right\|_2. \tag{15}$$

2.5. Correction for points in multiple grid cells

In fig. 2 the CPs in the given proximity (gray) are influenced by the compression of the point $(x,y)^T$. Image regions with

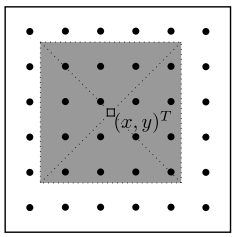

Fig. 2. One pixel (small square) influences 4×4 control points (black dots) in its proximity (gray square).

a strong compression, which spreads over multiple grid cells, might result in contradicting demands for the correcting values $d_{\boldsymbol{n}}^x$, $d_{\boldsymbol{n}}^y$ and $d_{\boldsymbol{n}}^z$. Solving the resulting system of linear equations with $3 \cdot N_x \cdot N_x \cdot N_x$ unknowns is computationally intensive. Instead we correct the CPs sequentially with an order determined by the sum of weights a_i contained in each grid cell. Each step reduces the degrees of freedom for the whole grid. Therefore the elements of the vectors $\boldsymbol{d}$ and $\boldsymbol{\theta}(\boldsymbol{u})$ can be separated depending on whether the values of $(d_{\boldsymbol{n}}^x, d_{\boldsymbol{n}}^y, d_{\boldsymbol{n}}^z)$ were already fixed or not. The elements are distributed to $\boldsymbol{d}_{\text{fixed}}$ resp. $\boldsymbol{d}_{\text{free}}$ and $\boldsymbol{\theta}_{\text{fixed}}$ resp. $\boldsymbol{\theta}_{\text{free}}(\boldsymbol{u})$. Eq. 11 is modified regarding the already fixed correction values

$$\boldsymbol{d}_{\text{fixed}}^T \cdot \boldsymbol{\theta}_{\text{fixed}}(\boldsymbol{u}) + \boldsymbol{d}_{\text{free}}^T \cdot \boldsymbol{\theta}_{\text{free}}(\boldsymbol{u}) \approx g(\boldsymbol{u}) \tag{16}$$

and the remaining degrees of freedom $\boldsymbol{d'}_{\text{free}}(\boldsymbol{u})$ are calculated

$$\boldsymbol{d'}_{\text{free}}(\boldsymbol{u}) = \frac{\left(g(\boldsymbol{u}) - \boldsymbol{d}_{\text{fixed}}^T \cdot \boldsymbol{\theta}_{\text{fixed}} \right) \cdot \boldsymbol{\theta}_{\text{free}}(\boldsymbol{u})}{\left| \boldsymbol{\theta}_{\text{free}}(\boldsymbol{u}) \right|^2}. \tag{17}$$

Correction values for each grid cell are determined by eq. 14.

3. RESULTS

For testing purposes an equidistant $32 \times 32 \times 32$ grid with spacing $\delta_x = \delta_y = \delta_z$ of 4 voxels is generated. A random translation is applied to each initial CP $\hat{\boldsymbol{\phi}}_{\boldsymbol{n}}$ for each direction separately by a maximum value of D_{max}. Therefore the random non-rigid transformation is given by

$$\tilde{\boldsymbol{\phi}}_{\boldsymbol{n}} = \hat{\boldsymbol{\phi}}_{\boldsymbol{n}} + D_{\text{max}} \cdot (\text{rand}_{[-1,1]}, \text{rand}_{[-1,1]}, \text{rand}_{[-1,1]})^T, \tag{18}$$

with $\text{rand}_{[-1,1]}$ returning a uniformly distributed random number between -1 and 1. In the range of the grid, N observation points $\boldsymbol{x}_i$, $\forall i = 1...N$ are randomly chosen. At these points the compression is eliminated by modifying the CPs.

The compression at the observed points is measured by the Jacobian determinant from eq. 1 at different steps of the algorithm: for the uncorrected registration, for the correction applied on each observed point individually (sect. 2.3), for the correction applied on all observed point in each grid cell individually (sect. 2.4), and finally for a global correction applied on all observed points (sect. 2.5). The resulting compressions and its variances are shown in fig. 3 for different numbers N of observed points.

Additionally the mean offset of $\|\boldsymbol{d'}_{\boldsymbol{n}}\|_2$, indicating the distortion of the initial registration, is shown in fig. 4 for different number N of observed points.

4. DISCUSSION

The compression rises with increasing deformation D_{max}, which is deducible by the different scaling of J_T axes in fig. 3. The point individual correction is, as implied by the algorithm, independent of N. It reliably eliminates varying compression and results in J_T of 1.004 resp. 1.01. The small constant offset to the desired value 1 might be caused by the asymmetric property of J_T [9]. The cell individual correction slightly inhibits the volume preservation as it is a compromise for all included points $\boldsymbol{x}_i$ which increases for higher

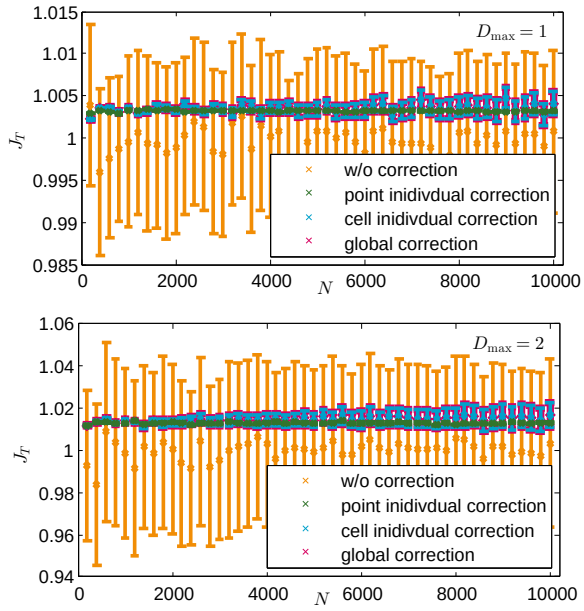

Fig. 3. Observed compression (crosses) and its variance (error bars) at different steps of the correction for different $D_{\max}$.

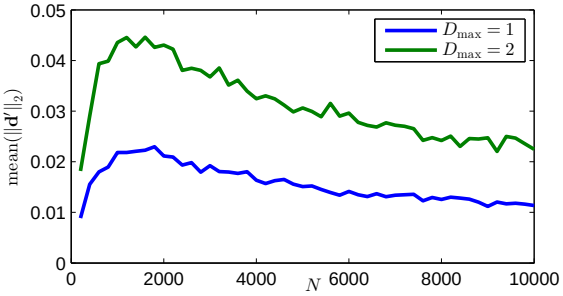

Fig. 4. Average offset for the control points after correction.

N. The global correction shows quasi identical results to cell individual correction.

The offset $\|\boldsymbol{d'_n}\|_2$ is higher for stronger deformations $D_{\max}$ as shown in fig. 4. It lies in the subvoxel range with less than 0.05 voxels and therefore only slightly distorts the initial registration. It first rises for increasing N because an increasing number of CPs is involved in the correction, while the not-involved CPs are not corrected ($\|\boldsymbol{d'_n}\|_2 = 0$). After peaking the mean offset falls with increasing N. This is caused by the compromise of the cell individual correction, which tends to small offsets. High offsets do not necessarily result in a worse registration compared to the initial registration, because the volume-preserving property might even result in a more suitable registration.

5. SUMMARY AND OUTLOOK

We described a non-iterative and reliable method to correct volume-distortion caused by free-form deformations. The compression variance is significantly reduced while the initial registration is only slightly modified. An evaluation, based on real medical images, exceed the scope of this paper. Still, simulations on high resolution 3D image data were performed and visually approved but not evaluated in detail. The extension from one point per grid cell to multiple points leads to an increasing compression variance. Other approaches for these extensions could be explored in the future. Also a simultaneous optimization of the CPs with respect to the feature points [7] and the compression should be investigated.

6. REFERENCES

[1] D. Rueckert, L. I. Sonoda, C. Hayes, D. L. G. Hill, M. O. Leach, and D. J. Hawkes, "Nonrigid registration using free-form deformations: Application to breast MR images," *IEEE TMI*, vol. 18, pp. 712–721, 1999.

[2] P. Faltin, K. Chaisaowong, T. Kraus, and T. Aach, "Markov-gibbs model based registration of CT lung images using subsampling for the follow-up assessment of pleural thickenings," in *IEEE ICIP*, 2011, vol. 18, pp. 2229–2232.

[3] P. Faltin, K. Chaisaowong, T. Kraus, and T. Aach, "Registration of lung surface proximity for assessment of pleural thickenings," in *Bildverarbeitung für die Medizin 2012*, 2012, pp. 213–218.

[4] E. Haber and J. Modersitzki, "Numerical methods for volume preserving image registration," *Inverse Problems*, vol. 20, pp. 1621–1638, 2004.

[5] T. Rohlfing, C. R. Maurer Jr., D. A. Bluemke, and M. A. Jacobs, "Volume-preserving nonrigid registration of mr breast images using free-form deformation with an incompressibility constraint," *IEEE TMI*, vol. 22, pp. 730–741, 2003.

[6] D. Loeckx, F. Maes, D. Vandermeulen, and P. Suetens, "Nonrigid image registration using free-form deformations with a local rigidity constraint.," in *MICCAI*, 2004, vol. 3216, pp. 639–646.

[7] S. Lee, G. Wolberg, and S. Y. Shin, "Scattered data interpolation with multilevel B-splines," *IEEE TVCG*, vol. 3, pp. 228–244, 1997.

[8] A. Rappoport, A. Sheffer, and M. Bercovier, "Volume-preserving free-form solids," *IEEE TVCG*, vol. 2, pp. 19–27, 1996.

[9] P. Cachier and D. Rey, "Symmetrization of the non-rigid registration problem using inversion-invariant energies: Application to multiple sclerosis.," in *MICCAI*, 2000, vol. 1935, pp. 472–481.